Communication: Anti-icing characteristics of superhydrophobic surfaces investigated by quartz crystal microresonators

Moonchan Lee, Changyong Yim, and Sangmin Jeon

Citation: The Journal of Chemical Physics **142**, 041102 (2015); doi: 10.1063/1.4906510
View online: http://dx.doi.org/10.1063/1.4906510
View Table of Contents: http://scitation.aip.org/content/aip/journal/jcp/142/4?ver=pdfcov
Published by the AIP Publishing

Communication: Anti-icing characteristics of superhydrophobic surfaces investigated by quartz crystal microresonators

Moonchan Lee, Changyong Yim, and Sangmin Jeon[a)]
Department of Chemical Engineering, Pohang University of Science and Technology (POSTECH), San 31 Namgu Hyojadong, Pohang 790-784, South Korea

(Received 28 December 2014; accepted 12 January 2015; published online 22 January 2015)

We investigated the anti-icing characteristics of superhydrophobic surfaces with various morphologies by using quartz crystal microresonators. Anodic aluminum oxide (AAO) or ZnO nanorods were synthesized directly on gold-coated quartz crystal substrates and their surfaces were rendered hydrophobic via chemical modifications with octyltrichlorosilane (OTS), octadecyltrichlorosilane (ODS), or octadecanethiol (ODT). Four different hydrophobic nanostructures were prepared on the quartz crystals: ODT-modified hydrophobic plain gold (C18-Au), an OTS-modified AAO nanostructure (C8-AAO), an ODS-modified AAO nanostructure (C18-AAO), and ODT-modified ZnO nanorods (C18-ZnO). The water contact angles on the C18-Au, C8-AAO, C18-AAO, and C18-ZnO surfaces were measured to be 91.4°, 147.2°, 156.3°, and 157.8°, respectively. A sessile water droplet was placed on each quartz crystal and its freezing temperature was determined by monitoring the drastic changes in the resonance frequency and Q-factor upon freezing. The freezing temperature of a water droplet was found to decrease with decreases in the water contact radius due to the decreases in the number of active sites available for ice nucleation. © *2015 AIP Publishing LLC.* [http://dx.doi.org/10.1063/1.4906510]

The freezing of a water droplet on solid surfaces is commonly observed on objects we encounter in our daily lives such as air conditioners, power transmission lines, refrigerators, and aircraft. The uncontrolled growth of frost layers on solid surfaces causes serious problems due to the additional thermal resistance, pressure drop, or drag force.[1–4] A number of methods have been developed for the de-icing and anti-icing of solid surfaces in recent decades. Conventional de-icing methods rely on the melting or breaking of ice, which requires energy. In contrast, anti-icing methods based on the development of ice-repellent coatings have attracted much attention recently because they prevent or reduce ice accumulation without requiring external energy.[5–7] Superhydrophobic surfaces are considered promising ice-repellent materials because of their nonwetting surface properties.[8–12] The low surface energy and poor heat transfer efficiency of superhydrophobic surfaces reduce ice adhesion and retard the freezing of water droplets on their surfaces.[13–17]

Most research into the anti-icing characteristics of superhydrophobic surfaces has used video microscopy to investigate the influence of their wettability and morphology on anti-icing performance.[18–24] Although it is simple and straightforward to monitor the freezing of a water droplet macroscopically, such optical techniques are not suitable for monitoring the phase changes on a surface between a water droplet and a substrate. The freezing of a water droplet on solid surfaces is a complicated process involving simultaneous mass and heat transfer. A sessile water droplet starts to freeze at the solid surface and gradually freezes in an upward direction because the heat transfer at the water-solid interface is more effective than in other regions of the droplet.[25,26] The freezing of a water droplet at the water-solid interface is affected by the morphology and wettability of the solid surface, but the freezing of an entire water droplet is affected not only by the surface characteristics but also by environmental factors such as air flow.

In this study, we used a quartz crystal microresonator (QCM) to investigate the influence of the morphology and wettability of superhydrophobic surfaces on the freezing temperature of a water droplet. The resonance frequency of a quartz crystal is sensitive to changes in mass and viscous damping only in the vicinity of its surface (~1 μm) because the acoustic wave decays rapidly with the distance from the surface,[27,28] which enables the sensitive evaluation of anti-icing performance. We synthesized anodic aluminum oxide (AAO) or ZnO nanorods directly onto gold-coated quartz crystal substrates and rendered their surfaces hydrophobic or superhydrophobic via chemical modifications with octyltrichlorosilane (OTS), octadecyltrichlorosilane (ODS), or octadecanethiol (ODT). The changes with temperature in the resonance frequencies and the Q-factors were measured for the surfaces with various wettabilities and morphologies. This study, to the best of our knowledge, presents the first application of QCMs to the investigation of the anti-icing performances of hydrophobic and superhydrophobic surfaces.

For the preparation of a porous AAO nanostructure on a quartz crystal, a high purity Al film was deposited (2 μm) on the quartz crystal substrate and a two-step anodization process was conducted as described elsewhere.[27,29] In brief, the Al film was anodized in a 0.3 M oxalic acid solution at 15 °C by applying 40 V for 10 min. Then, the irregularly grown

a)Author to whom correspondence should be addressed. Electronic mail: jeons@postech.ac.kr

aluminum oxide layer was selectively removed by immersing the substrate in a mixture of phosphoric acid (5 wt. %) and chromic acid (2 wt. %) at 60 °C for 10 min. The resulting Al film with dimple structures was anodized again under the same conditions for 10 min to produce an aluminum oxide layer with ordered nanopores. The average pore diameter was increased to 80 nm by incubation in a 0.1 M phosphoric acid solution at 30 °C for 60 min. For the preparation of ZnO nanorods on a quartz crystal, 30 nm thick ZnO seed layers were deposited on a quartz crystal substrate and ZnO nanorods were hydrothermally grown on the coated quartz crystal at 90 °C for 75 min in a 10 mM $Zn(NO_3)\cdot 6H_2O$ solution at a pH of 10.6.[30]

The anti-icing performances of various nanostructured quartz crystal substrates were assessed by measuring the changes in the resonance frequencies and Q-factors with decreases in temperature. The Q-factor of a quartz crystal resonator is defined as the ratio of the energy stored to the energy dissipated per cycle and is inversely proportional to the dissipation factor. Each nanostructured quartz crystal was placed inside a jacketed glass beaker that was connected to a refrigerated circulating bath (JEIO Tech, Korea) containing ethanol as a coolant. The temperature of the quartz crystal substrate was measured with a thermocouple attached to the quartz crystal holder. A 2 μl water droplet was placed on the quartz crystal substrate at 5 °C and the temperature was gradually decreased to −10 °C (see Figure S1 in the supplementary material for the temperature profile).[31] The temperature-dependent changes in the resonance frequency and Q-factor of the quartz crystal were monitored *in situ* by connecting the electrodes to a custom-built PC-based conductance measurement system.[28] The resonance frequencies and Q-factors were calculated from Lorentzian fits of the conductance spectra. The water contact angle of each nanostructure surface was measured by using a goniometer (SmartDrop, Femtofab, Korea) with a 2 μl water droplet.

ZnO nanorods or AAO nanostructures were synthesized directly onto quartz crystal substrates. Figure 1(a) shows a scanning electron microscopy (SEM) image of a porous AAO nanostructure. The mean pore diameter, pore-to-pore distance, and thickness of the AAO nanostructure were measured to be 80 nm, 100 nm, and 1.2 μm, respectively. ZnO nanorods were grown directly on a quartz crystal substrate by using the hydrothermal method, and the height, diameter, and rod-to-rod distance of the resulting ZnO nanorods were found to be 1.2 μm, 90 nm, and 100 nm, respectively (Figure 1(b)). The insets in Figures 1(a) and 1(b) show optical microscopy images of the quartz crystal surfaces with an AAO nanostructure and ZnO nanorods, respectively. The diameter of each nanostructure pattern is 1.27 cm. In addition to these nanostructured quartz crystal substrates, a conventional gold-coated quartz crystal was prepared to investigate the influence of surface morphology on anti-icing performance.

The surfaces of the quartz crystals with AAO nanostructures and ZnO nanorods were chemically modified to render them hydrophobic by incubating them in 10 mM OTS, 10 mM ODS, or 10 mM ODT for 3 h. Thiol-functionalization (ODT) was applied to the ZnO nanorods and the gold surface whereas silane-functionalization (OTS and ODS) was applied to the AAO nanostructures. Four different hydrophobic or superhydrophobic surfaces were prepared: ODT-modified plain gold (C18-Au), an OTS-modified AAO nanostructure (C8-AAO), an ODS-modified AAO nanostructure (C18-AAO), and ODT-modified ZnO nanorods (C18-ZnO). Although it was reported that the surfaces coated with alkylsilane gradually lost their ice repellency upon repeated icing/deicing cycles,[32] negligible changes in the ice repellency were observed during the experimental period. The water contact angles were measured at eight different locations on the C18-Au, C8-AAO, C18-AAO, and C18-ZnO substrates and found to be 91.4 ± 1.5°, 147.2 ± 0.5°, 156.8 ± 0.7°, and 157.5 ± 0.7°, respectively, as shown in Figures 2(a)-2(d). In contrast to the hydrophobic surfaces, a plain gold-coated quartz crystal substrate was found after UV irradiation for 20 min (UV-Au) to exhibit hydrophilic characteristics with a water contact angle of 10.7 ± 2.5°. C18-Au, C18-AAO, and C18-ZnO were compared to investigate the effects of surface morphology on anti-icing performance whereas C8-AAO and C18-AAO were compared to investigate the effects of surface wettability.

The wettabilities of the quartz crystal surfaces were investigated by placing a 2 μl water droplet on each quartz substrate and measuring the change in the resonance frequency. Figure 2(e) shows the variation in the resonance frequency upon placement of a 2 μl water droplet on each quartz crystal substrate. The change in the mass of a quartz crystal is directly related to the change in the resonance frequency according to the Sauerbrey equation,[33]

$$\Delta m = -\frac{A\sqrt{\rho_q \mu_q}}{2{f_0}^2}\Delta f, \tag{1}$$

where A (cm^2) is the active area of the quartz crystal, ρ_q (2.648 g/cm^3) is the density of quartz, f_0 is the resonance frequency of the unloaded quartz crystal, and μ_q (2.947×10^{11} $g/(cm\ s^2)$) is the shear modulus of quartz. The frequency change was not converted to a mass change here because only a small portion of the quartz crystal substrate was

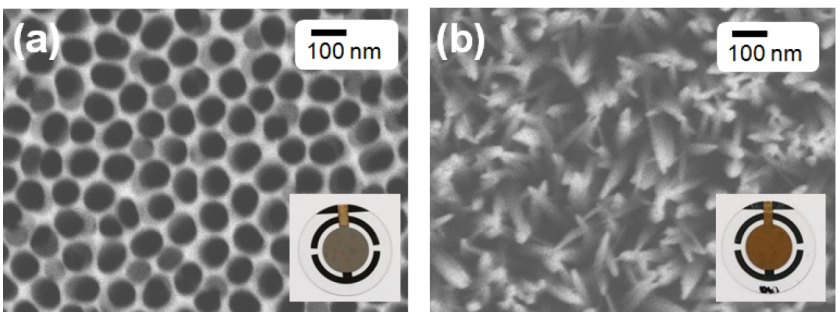

FIG. 1. SEM images of (a) an AAO nanostructure and (b) ZnO nanorods. The insets show optical microscopy images of the quartz crystal microresonators with each nanostructure. The diameter of the nanostructure pattern on the quartz crystal substrate is 1.27 cm.

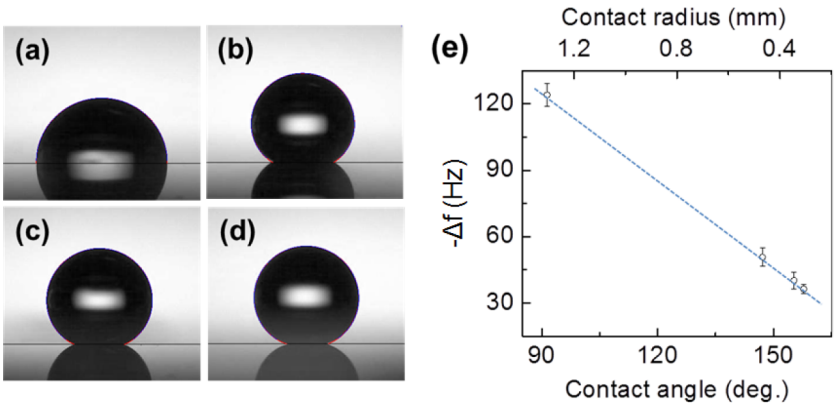

FIG. 2. Optical microscopy images of water droplets on (a) C18-Au, (b) C8-AAO, (c) C18-AAO, and (d) C18-ZnO. (e) Variation in the resonance frequency with contact radius or contact angle due to the loading of a 2 μl water droplet onto the various quartz crystal substrates.

covered with a water droplet. However, it is safe to assume that the frequency change correlates qualitatively with the mass change. The frequency change upon the placement of a water droplet decreases with increases in the water contact angle (i.e., with decreases in the water contact radius). This trend arises because the resonance frequency of a quartz crystal vibrating in a thickness shear mode is affected only by the mass change near the surface. The decay length of the shear wave of a quartz crystal immersed in a fluid is given by

$$\delta = \left(\frac{\eta_l}{\pi f \rho_l}\right)^{\frac{1}{2}}, \tag{2}$$

where f is the resonance frequency of the quartz crystal, ρ_l and η_l are the density and viscosity of the surrounding fluid, respectively. The decay length of the shear wave of a 5 MHz quartz crystal in water at 25 °C is only ~240 nm, so the frequency change is affected not by the entire mass of the water droplet on the quartz crystal but only by the mass of the water near the surface, which is proportional to the contact radius (or contact area).[27] The contact radius of the water droplets on the quartz crystals increases in the following order (which is the order of decreasing contact angle): C18-ZnO (0.33 ± 0.02 mm) < C18-AAO (0.35 ± 0.02 mm) < C8-AAO (0.45 ± 0.05 mm) < C18-Au (1.31 ± 0.08 mm) < UV-Au (5.52 ± 0.57 mm). As a result, the largest decrease in resonance frequency upon the placement of a 2 μl water droplet was observed for the hydrophilic UV-Au due to its largest contact radius.

To investigate the influence of the surface morphology or surface wettability on the anti-icing performance, each quartz crystal substrate with a 2 μl water droplet on its center was placed inside a jacketed glass beaker and the changes in the resonance frequency and Q-factor (which is inversely proportional to the full width at half maximum of the peak) with decreasing temperature were monitored. Figure 3 shows the conductance spectra of C18-Au at three different temperatures during cooling from 5 °C to −10 °C. The resonance frequency decreases upon the placement of a water droplet due to the increase in mass loading (black to red). A further decrease in the resonance frequency was observed during cooling (red to blue), which is attributed to the gradual condensation of water vapor. A control experiment was conducted on C18-Au without the addition of a water droplet and a similar decrease in the resonance frequency was observed, which indicates that this frequency decrease is caused by the condensation of water vapor (see Figure S2 in the supplementary material).[31] It is interesting to note that a dramatic increase in the frequency is evident upon the freezing of the water droplet (blue to green). The water droplet is viscously coupled with the quartz surface and vibrates out-of-phase with the substrate (i.e., the decay length is relatively small) whereas the ice droplet is elastically coupled with the quartz surface and vibrates in-phase with the substrate (i.e., the decay length is relatively large). Further, the optical microscopy image of a water droplet shows that the contact radius after freezing is larger than that before freezing due to the volume expansion upon freezing. As a result, the phase transition from water to ice is expected to cause a decrease in the resonance frequency. The abnormally large increase in the resonance frequency upon the freezing of the water droplet is attributed to changes in the surface stress of the quartz crystal substrate. The increase in the contact radius during the freezing of the water droplet induces an increase in the surface stress of the quartz crystal, which increases the resonance frequency and decreases the Q-factor of the quartz crystal.[34,35]

Figures 4(a) and 4(b) show the temperature-dependent changes during cooling in the resonance frequencies and Q-factors, respectively, of various quartz surfaces with a water

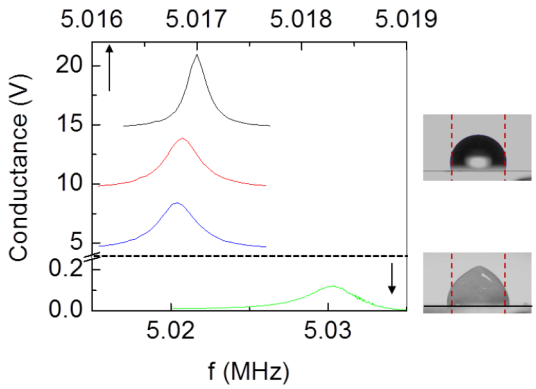

FIG. 3. Conductance spectra of C18-Au: without a water droplet at 5 °C (black), with a 2 μl water droplet at 5 °C (red), right before freezing of the water droplet (blue), and right after freezing of the water droplet (green). Note that the scales on the top x-axis and the upper y-axis for the three peaks (black, red, and green) are different from the scales on the bottom x-axis and the lower y-axis for the green peak. The optical microscopy images show a water droplet on C18-Au before and after freezing.

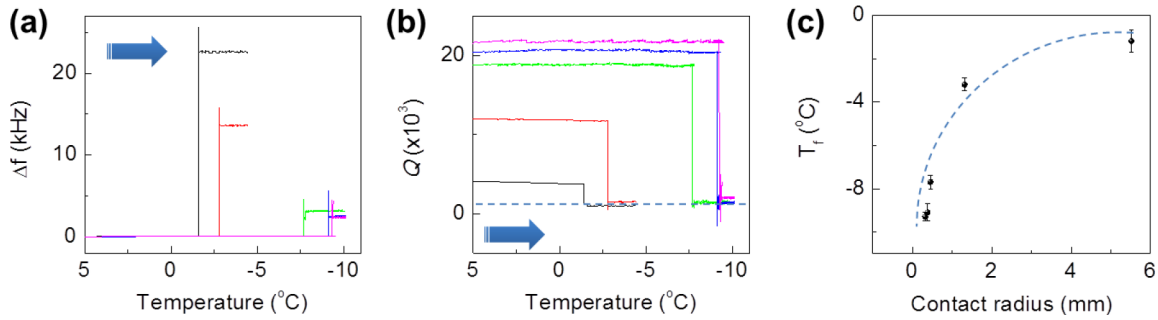

FIG. 4. Variations with the decreasing temperature in (a) the resonance frequencies and (b) the Q-factors of various quartz crystal substrates: UV-Au (black), C18-Au (red), C8-AAO (green), C18-AAO (blue), and C18-ZnO (magenta). (c) Variation in the freezing temperature (T_f) of a water droplet on various quartz substrates as a function of the water contact radius. The curve was inserted as a guide.

droplet. The sharp changes in the resonance frequency and Q-factor upon freezing enable the determination of the freezing temperature of a water droplet on each surface. The freezing temperature of the water droplet on each surface decreases in the order UV-Au (-1.2 ± 0.5 °C), C18-Au (-3.2 ± 0.3 °C), C8-AAO (-7.7 ± 0.3 °C), C18-AAO (-9.1 ± 0.4 °C), and C18-ZnO (-9.3 ± 0.2 °C) as shown in Figure 4(c), which indicates that the freezing temperature decreases with increasing water contact angle due to the decreased number of active sites for ice nucleation. Note that the freezing temperature measured using QCMs does not represent the temperature for the freezing of the entire water droplet but rather the temperature for the freezing of the water at the water-solid interface because the frequency changes of QCMs are only sensitive to regions near the surface. The changes in the resonance frequency at the freezing temperature decrease with increasing water contact angle (i.e., with decreasing water contact radius) whereas the changes in the Q-factor at the freezing temperature increase with increasing water contact angle. This trend arises because the freezing of a water droplet with a small water contact radius induces smaller increases in the surface stress of the quartz crystal and the initial Q-factor of the quartz crystal with a small water contact radius (i.e., less viscous damping) is larger than that with a large water contact radius.

We used quartz crystal microresonators to investigate the influence of surface wettability and surface morphology on the anti-icing performances of various surfaces. Five different structures were prepared directly on quartz crystal microresonators including UV-Au, C18-Au, C8-AAO, C18-AAO, and C18-ZnO. Their surface wettability varied from hydrophilic to superhydrophobic due to different chemical modifications and surface morphologies. The freezing of sessile water droplets on the quartz crystals was found to induce drastic changes in their resonance frequencies and Q-factors due to the changes in surface stress upon freezing. We found that C18-ZnO exhibited the best anti-icing performance (i.e., the lowest freezing temperature), which arises because its water contact radius (i.e., the number of active sites available for ice nucleation) is the smallest.

This research was supported by a Grant No. 14CTAP-C077604-01 funded by Ministry of Land, Infrastructure, and Transport of Korean government.

[1]L. O. Andersson, C. G. Golander, and S. Persson, J. Adhes. Sci. Technol. **8**, 117 (1994).
[2]J. L. Laforte, M. A. Allaire, and J. Laflamme, Atmos. Res. **46**, 143 (1998).
[3]R. W. Gent, N. P. Dart, and J. T. Cansdale, Philos. Trans. R. Soc., A **358**, 2873 (2000).
[4]S. Frankenstein and A. M. Tuthill, J. Cold Reg. Eng. **16**, 83 (2002).
[5]Y. He, C. Jiang, S. Wang, Y. Hao, J. Xie, X. Cao, W. Tan, and W. Yuan, ACS Appl. Mater. Interfaces **6**, 18063 (2014).
[6]R. Ramachandran and M. Nosonovsky, Soft Matter **10**, 7797 (2014).
[7]X. Li, Y. Zhao, and X. Yuan, Appl. Surf. Sci. **316**, 222 (2014).
[8]L. Cao, A. K. Jones, V. K. Sikka, J. Wu, and D. Gao, Langmuir **25**, 12444 (2009).
[9]M. Ruan, W. Li, B. Wang, B. Deng, F. Ma, and Z. Yu, Langmuir **29**, 8482 (2013).
[10]S. Jung, M. Dorrestijn, D. Raps, A. Das, C. M. Megaridis, and D. Poulikakos, Langmuir **27**, 3059 (2011).
[11]P. Tourkine, M. L. Merrer, and D. Quéré, Langmuir **25**, 7214 (2009).
[12]S. A. Kulinich, S. Farhadi, K. Nose, and X. W. Du, Langmuir **27**, 25 (2011).
[13]S. Farhadi, M. Farzaneh, and S. A. Kulinich, Appl. Surf. Sci. **257**, 6264 (2011).
[14]T. Bharathidasan, S. V. Kumar, M. S. Bobji, R. P. S. Chakradhar, and B. J. Basu, Appl. Surf. Sci. **314**, 241 (2014).
[15]X. Zhan, Y. Yan, Q. Zhang, and F. Chen, J. Mater. Chem. A **2**, 9390 (2014).
[16]J. Lv, Y. Song, L. Jiang, and J. Wang, ACS Nano **8**, 3152 (2014).
[17]Y. Wang, J. Xue, Q. Wang, Q. Chen, and J. Ding, ACS Appl. Mater. Interfaces **5**, 3370 (2013).
[18]M. He, J. Wang, H. Li, X. Jin, J. Wang, B. Liu, and Y. Song, Soft Matter **6**, 2396 (2010).
[19]M. He, J. Wang, H. Li, and Y. Song, Soft Matter **7**, 3993 (2011).
[20]D. P. Singh and J. P. Singh, Appl. Phys. Lett. **102**, 243112 (2013).
[21]P. Hao, C. Lv, and X. Zhang, Appl. Phys. Lett. **104**, 161609 (2014).
[22]L. Boinovich, A. M. Emelyaneko, V. V. Korolev, and A. S. Pashinin, Langmuir **30**, 1659 (2014).
[23]F. Arianpour, M. Farzaneh, and S. A. Kulinich, Appl. Surf. Sci. **265**, 546 (2013).
[24]Q. Hao, Y. Pang, Y. Zhao, J. Zhang, J. Feng, and S. Yao, Langmuir **30**, 15416 (2014).
[25]Q. Zhang, M. He, J. Chen, J. Wang, Y. Song, and L. Jiang, Chem. Commun. **49**, 4516 (2013).
[26]Q. Zhang, M. He, X. Zeng, K. Li, D. Cui, J. Chen, J. Wang, Y. Song, and L. Jiang, Soft Matter **8**, 8285 (2012).
[27]M. Lee, C. Yim, and S. Jeon, Langmuir **30**, 7931 (2014).
[28]W. Ko, N. Jung, M. Lee, M. Yun, and S. Jeon, ACS Nano **7**, 6685 (2013).
[29]M. Lee, D. Lee, N. Jung, M. Yun, C. Yim, and S. Jeon, Appl. Phys. Lett. **98**, 013107 (2011).
[30]Y. Tak and K. Yong, J. Phys. Chem. B **109**, 19263 (2005).
[31]See supplementary material at http://dx.doi.org/10.1063/1.4906510 for temperature profiles of a quartz crystal during cooling.
[32]S. A. Kulinich, M. Honda, A. L. Zhu, A. G. Rozhin, and X. W. Du, "The icephobic performance of alkyl-grafted aluminum surfaces," Soft Matter (published online).
[33]G. Z. Sauerbrey, Z. Phys. **155**, 206 (1959).
[34]E. P. Eernisse, J. Appl. Phys. **43**, 1330 (1972).
[35]L. Tan, Q. Xie, X. Jia, M. Guo, Y. Zhang, H. Tang, and S. Yao, Biosens. Bioelectron. **24**, 1603 (2009).